

Climbing four tops with graph networks, transformers and pairwise features

Luc Builtjes^a Sascha Caron^{a,b} Polina Moskvitina^{a,b} Clara Nellist^{b,c} Roberto Ruiz de Austri^d Rob Verheyen^e Zhongyi Zhang^{a,b}

^aHigh Energy Physics, Radboud University Nijmegen, Heyendaalseweg 135, 6525 AJ Nijmegen, the Netherlands

^bNikhef, Science Park 105, 1098 XG Amsterdam, the Netherlands

^cInstitute of Physics, University of Amsterdam, 1090 GL Amsterdam, The Netherlands

^dInstituto de Física Corpuscular, IFIC-UV/CSIC, Valencia, Spain

^eDepartment of Physics and Astronomy, University College London, London, WC1E 6BT, UK

E-mail: scaron@nikhef.nl, p.moskvitina@nikhef.nl, c.nellist@nikhef.nl,
rruiz@ific.uv.es, r.verheyen@ucl.ac.uk, zhang@nikhef.nl

ABSTRACT: The ATLAS and CMS collaborations at CERN aim to measure the production of four top quarks in a single LHC collision. The sensitivity to this process is heavily reliant on the classification accuracy of these events in relation to the vast background from other Standard Model processes. The four top process is thus a prime candidate for the implementation and comparison of more advanced classification techniques based on deep learning, rather than the commonplace traditional methods. In this paper, we present a data set and comparison of a variety of methods that have recently emerged. We find that a transformer architecture (Particle Transformer) and a graph neural network (Particle Net), with the inclusion of pairwise features, perform best. Compared to the performance of a baseline boosted decision tree, the improvement in signal efficiency equates to a gain of 30 – 50% in integrated luminosity.

Contents

1	Introduction	1
2	Data Description	2
2.1	Data generation	2
2.2	Event and object selection	2
2.3	Data format	3
3	Machine learning models	4
3.1	Boosted decision tree	4
3.2	Fully-connected network	5
3.3	Convolutional network	5
3.4	Particle Net	5
3.5	Particle Transformer	6
3.6	Pairwise features	6
4	Results	7
5	Conclusions	8

1 Introduction

The top quark is the most massive known fundamental particle, and it is therefore potentially highly sensitive to effects of new physics outside the Standard Model (SM). With the unprecedented amount of data provided by the second operational run of the Large Hadron Collider (LHC), one can now start to measure rare processes with very small cross sections, such as the production of four top quarks originating from a single proton-proton collision event (4tops). Enhancements of very rare SM cross sections from new physics through the production of heavy objects in association with a top-quark pair are possible in a number of different proposed models, see e.g. [1].

The SM 4tops process is an excellent testbed for supervised machine learning (ML) searches for rare signals. At the time of writing (November 2022), the expected significance for 4tops production in the ATLAS and CMS experiment is 2.6 [2] and 2.7 [3] standard deviations, respectively. After preselecting candidate events, the 4top analysis proceeds to an event classification step via a boosted decision tree (BDT) based on TMVA [4] in signal (events with 4 tops) and background (events stemming from all other SM processes). Sensitivity is calculated using a fit of signal and background templates to the BDT output distribution (ranging from 0 for background-like to 1 for signal-like events). Details of the analysis procedure can be found in References [1] and [3]. A slight, as of yet inconclusive, excess of data has been observed [1] and the 4tops signal has not yet met the criteria for observation (i.e. 5 sigma significance of a signal relative to the background hypothesis). Improving the sensitivity to 4top events and comparing the measured cross-section for 4tops production with the SM prediction is currently a primary goal of the LHC community.

At the same time, the recent deep learning revolution has found a large variety of applications in high energy physics (see e.g. [5] for a review). One of these is the development of a large variety of architectures for the purpose of classification of particle physics data, including improved BDTs [6], convolutional networks [7], graph neural networks [8] and attention-based architectures [9, 10]. These methods are mainly used in the context of the classification of jet data. On the other hand, their application to event-level data has not yet been explored to the same degree, and BDTs are still the most commonly used method.

In this work, we present a publicly available dataset to test classification methods for 4top events. We then apply a series of different classifications methods to this data set. To the best of our knowledge, the more sophisticated of these methods have not been compared on event-level data. We perform wide hyperparameter scans over all models and compute several figures of merit to evaluate their performance. We find that the two equally best performing methods are based on graph neural networks and transformer architectures, supplemented by the inclusion of pairwise features beyond the raw four-vector data.

In Section 2 we describe the data generation and the data format. Section 3 briefly describes the Machine Learning models used in the comparison and their optimization. We discuss our results in Section 4 and conclusions in Section 5.

2 Data Description

In this section, we describe the data generation and the data format used for this work.

2.1 Data generation

We simulated proton-proton collisions at a center-of-mass energy of 13 TeV. Our background data consists of the irreducible backgrounds $t\bar{t} + X$, where $X = Z, W^+, H$ and W^+W^- , while the signal is four tops. The hard scattering process generation was performed at leading order, where up to two additional jets are added to the final state in the case of the background processes, and up to one for the signal. The cross sections for all the processes and the corresponding total number of events generated are depicted in Tab. 1.

The hard scattering was generated with **MG5_aMC@NLO** version 2.7 [11] with the **NNPDF31_lo** parton distribution functions set [12], using the 5 flavor scheme. Parton showering was performed with **Pythia** version 8.239 [13], while the MLM merging scheme [14] was used to merge high-multiplicity hard scattering events with the parton shower. A fast detector simulation was performed with **Delphes** version 3.4.2 [15] using the ATLAS detector map. Finally, an $H_T = \sum_{jets} E_T > 400$ GeV restriction was imposed at the parton level during event generation. The purpose of this restriction is generation efficiency, since our signal region imposes $H_T > 500$ GeV on the reconstructed objects (see Section 2.2 for details.).

2.2 Event and object selection

Collision events consist of objects such as jets, b-jets, leptons, and photons, each with their corresponding kinematic variables (see Section 2.3). Following the strategy in Reference [16], an event is saved if at least one of the following conditions is met:

- At least one jet or a b -jet with transverse momentum $p_T > 60$ GeV and pseudorapidity $|\eta| < 2.8$,
- At least one electron with $p_T > 25$ GeV and $|\eta| < 2.47$, except for $1.37 < |\eta| < 1.52$,

Physics process	σ (pb)	N_{tot}	ϵ
$pp \rightarrow t\bar{t}t\bar{t}$ (+1 j)	0.01	32463742	0.007
$pp \rightarrow t\bar{t}h$ (+2 j)	0.022	29783343	0.001
$pp \rightarrow t\bar{t}W^\pm$ (+2 j)	0.045	8954246	0.005
$pp \rightarrow t\bar{t}W^+W^-$ (+2 j)	0.0096	20160377	0.003
$pp \rightarrow t\bar{t}Z$ (+2 j)	0.034	10605846	0.011

Table 1. Irreducible background processes (first column) plus the 4tops signal with the corresponding LO cross section σ in pb (second column), the total number of generated events N_{tot} (third column) and the efficiency ϵ of the cuts applied (fourth column).

- At least one muon with $p_T > 25$ GeV and $|\eta| < 2.7$,
- At least one photon with $p_T > 25$ GeV and $|\eta| < 2.37$.

The subsequent object selection then follows Ref. [1], meaning that individual objects are kept only if they pass the following requirements:

- Electron candidates satisfying $p_T > 28$ GeV and $|\eta| < 2.47$ are selected. In the region $1.37 < |\eta| < 1.52$, known as the LAr crack region, electrons are rejected in order to reduce the contribution from non-prompt and fake electrons due to detector design in the liquid Argon calorimeter.
- Muon candidates are required to pass the Medium quality working point, with $p_T > 28$ GeV, and $|\eta| < 2.5$.
- Jet candidates satisfying $p_T > 25$ GeV and $|\eta| < 2.5$ are selected.

Finally to remove as much background as possible with respect to the signal, we define a signal region [1] that requires at least six jets, at least two of which are b-tagged, $H_T > 500$ GeV, and two leptons of the same sign, or at least three leptons for each event. The resulting efficiencies are shown in Table 1.

2.3 Data format

The generated Monte Carlo data were saved as ROOT files and then processed into CSV files using the event selection presented in Section 2.2. Each line in the CSV files is of variable length and contains three event specifiers followed by the kinematic features for each object in the event. The specific line format follows the event format used in the Dark Machines challenges [17, 18], given by

event ID; process ID; weight; MET; METphi; obj1, E1, pt1, eta1, phi1; obj2, E2, pt2, eta2, phi2;..

such that each object is represented by a string that starts with an identifier *objn*¹, followed by its kinematic properties in the form of a four-vector containing the full energy E and the transverse momentum p_T in units of MeV, as well as the pseudo-rapidity η and the azimuthal angle ϕ . The other relevant quantities are *MET* and *METphi*, which represent the magnitude of the E_T^{miss} and the azimuthal angle $\phi_{E_T^{\text{miss}}}$ of the missing transverse energy. The other three components represent the identity of an event, the corresponding physical process, and the event weight, which is given by the cross section of the process divided by the total number of events generated.

¹j: jet, b: b-jet, e: electron, e+: positron, μ -: muon, μ +: antimuon, g: photon.

Since the length of the events is variable, the data is zero-padded to the largest number of objects found in the events within in the entire dataset. The dataset includes 302 072 events, half of which correspond to the four tops signal and half of which are background processes. All background processes have an equal number of events. Finally the dataset was split in 80 % used for training, 10 % used for validation and 10 % used for testing. The data are available in CSV format in [19].

3 Machine learning models

In this section we provide a brief summary of the models used in this work.

3.1 Boosted decision tree

We use Light Gradient Boosting Machine (LightGBM²) for this study to test the performance of Boosted Decision Tree (BDT).

BDTs combine a series of weak classifiers (decision trees) into a stronger classifier through gradient boosting. The boosting strategy is defined with respect to a series of previous decision trees f_1, f_2, \dots, f_{t-1} which remain fixed, while the t -th tree f_t is calculated. This process is made highly efficient in LightGBM by converting the input data to histograms, and using gradient based sampling to focus on the data that are not well modelled. This procedure reduces memory usage and is optimized for both CPU and GPU performance. LightGBM uses first- and second-order derivatives to minimize the loss for the next iteration for gradient boosting

$$\begin{aligned} \text{Loss}^{(t)} &= \sum_{i=1}^n l(y_i, (\hat{y}_i^{(t-1)} + f_t(x_i))) + \sum_{i=1}^t \omega(f_i) \\ &\approx \sum_{i=1}^n [g_i f_t(x_i) + \frac{1}{2} h_i f_t^2(x_i)] + \omega(f_t) + \text{constant} \\ g_i &= \partial_{\hat{y}_i^{(t-1)}} l(y_i, \hat{y}_i^{(t-1)}), \quad h_i = \partial_{\hat{y}_i^{(t-1)}}^2 l(y_i, \hat{y}_i^{(t-1)}). \end{aligned} \quad (3.1)$$

where l is a reconstruction loss functions, e.g. Mean Square Error, Binary Cross Entropy, etc., f_t is the t -th tree, and $\hat{y}^{(t-1)}$ is the class label predicted by f_1, f_2, \dots, f_{t-1} . The term $\omega(f_i)$ represents tree complexity terms that involve properties such as depth, number of leaves, etc. LightGBM uses a depth-first algorithm to add branches to the tree f_t with limitation on largest depth while minimizing Equation (3.1).

A common property of collision data in particle physics is a wide variability in object numbers and types. A structured formatting of the data would thus lead to a large degree of sparsity, which we found to significantly degrade the BDT performance. We thus choose to pre-process the data by limiting the maximum number of (jets, b-jets, e^- , e^+ , μ^- , μ^+) to the (4, 4, 1, 1, 1, 1) hardest objects respectively.

One useful feature of this BDT is the fact that training is much faster than is the case for all the other architectures described below. Therefore, fine tuning of the hyper parameters and adjustment of the data format is easy and efficient. Another attractive advantage of BDTs is their capacity to indicate feature importance, which details which input value is most important for its performance. In Section 3.6 we discuss the inclusion of high-level features beyond the raw four-vectors, where this feature is especially useful.

²<http://github.com/microsoft/LightGBM> with `binary cross entropy` as loss function, `auc` as early stop metric, 5000 estimators, 500 leaves, 0.01 learning rate, `gbdt` boost type, and max depth equaling to 15.

Variables
$E, p_T, \eta, \phi, \text{jet}_{\text{tag}}, \text{b-jet}_{\text{tag}}, e_{\text{tag}}^-, e_{\text{tag}}^+, \mu_{\text{tag}}^-, \mu_{\text{tag}}^+, \gamma_{\text{tag}}$

Table 2. Particle input variables for the 1D CNN, Particle Net and Particle Transformer.

3.2 Fully-connected network

Fully-connected neural networks (FCNs) [20] are deep neural networks in their most basic form. They consist of several layers of neurons, each of which is connected to every neuron in the following layer. The connections represent a linear transformation with trainable parameters, which are followed by a non-linear activation function. After the final layer with a single node, a sigmoid activation is applied to produce a classification score.

The hidden layers all use ReLU activations, and the first five layers were followed by a Dropout layer with probability 0.5. The network was trained with the Adam optimizer [21] with default parameters. An exponential learning rate schedule with $\gamma = 0.95$ was used, as well as early stopping by monitoring the performance on the validation set. The batch size and learning rates, as well as the network parameters were optimized using Optuna [22].

As is the case for BDTs, we found that the FCN performance generally deteriorates when applied to large, sparse input data. The data is thus pre-processed following the prescription given in Section 3.1.

3.3 Convolutional network

Convolutional Neural Networks (CNNs) [23] are mainly applied to analyze data where adjacent items have a causal relationship, i.e. image data. CNNs apply convolutional operations through trainable filter matrices that slide over the data to produce output that is translationally equivariant. The convolutional layers are usually followed by pooling operations to reduce the dimension of the data in the inner network layers. Here, we utilize a one-dimensional variant of such an architecture (1D CNN) called the DeepAK8 algorithm, originally used for jet tagging [24].

We incorporate 11 particle features as given in Table 2. Each feature is then represented by an array of size $N_{\text{max}} = 19$, the maximum number of objects in an event. The event-wide features E_T^{miss} and $\phi_{E_T^{\text{miss}}}$ are added to the p_T and ϕ feature vectors respectively. Following [24], the network consists of a set of 1D convolutional blocks that pass over each of the feature vectors separately. The output of these blocks is concatenated and passed to a FCN with ReLU activations. The blocks are composed of two sub-blocks which consist of a set of convolutional layers with a ReLU activation function followed by a max pooling layer and a Dropout layer with dropout probability 0.2. The model was trained with the Adam optimizer with default parameters, with a learning rate scheduler and early stopping which both monitor the validation AUC to prevent overfitting. The number of convolutional layers, the number of filters and the kernel size, as well as the FCN parameters were optimized with Optuna.

3.4 Particle Net

Particle Net (PN) [25] is a graph-based architecture based on Dynamic Graph Convolutional Neural Networks [26]. It treats events as particle cloud inspired by a point cloud [26] in Computer Vision challenges. Every final-state particle, encoded by the variables shown in Table 2, is represented by an individual node in the graph, carrying (E, p_T, η, ϕ) as node values. Edges are constructed by connecting these particles with their k-nearest neighbours (kNN), where distances are defined as

$\Delta R_{ij} = \sqrt{(\Delta\eta)_{ij}^2 + (\Delta\phi)_{ij}^2}$. The graph representing the event thus has N (number of final state particles) nodes and kN edges.

Messages are passed to every node i by all k neighbouring nodes j in the graph by applying the operation

$$x'_i = \frac{1}{k} \sum_{j=1}^k \text{FCN}(x_i, x_i - x_{i_j}) \quad (3.2)$$

to every node. Here, j runs over the k nearest neighbors of i and the weights of the FCN are the same for every node and edges combination. We performed experiments with an attention-weighted procedure rather than the simple averaging over edges of Equation (3.2), but found no difference in performance.

The node features are then updated to x'_i . Multiple layers of the above procedure are applied consecutively, and the node features after every step are concatenated, averaged over the nodes, and then processed by another FCN which also receives the E_T^{miss} and $\phi_{E_T^{\text{miss}}}$ to obtain a classification.

We performed a wide hyperparameter scan over the ParticleNet architecture and found no significant difference in performance as long as sufficient capacity is available. We thus choose to use the hyperparameter settings recommended in [25] and the training procedure of [27]. Our implementation is based on [28].

3.5 Particle Transformer

Particle Transformer (ParT) [10] is a transformer-based architecture originally developed for jet tagging. It is inspired by the success of similar architectures in fields such as natural language processing [29], embedding individual particles rather than words. At its core lies the repeated application of the self-attention mechanism

$$\text{Attention}(Q, K, T) = \text{SoftMax} \left(QK^T / \sqrt{d} \right) V, \quad (3.3)$$

where Q , K and V are trainable d -dimensional linear projections of the particle embedding based on the variables of Table 2.

The application of the attention mechanism serves to correlate every particle with all others. Furthermore, it is applicable to varying numbers of particles and is explicitly permutation invariant. Classification is obtained by appending a classification token to the list of particle embeddings before the last few layers of the transformer. This token is a trainable set of weights that is identical for every event³. The attention mechanism then correlates the classification token with the event, after which it is processed by an FCN, which also receives E_T^{miss} and $\phi_{E_T^{\text{miss}}}$, to produce a classification label. Our implementation is based on [31].

As was the case for Particle Net, a hyperparameter scan over the ParT architecture does not lead to significant differences in performance. We thus choose to use the hyperparameter settings and training procedure recommended in [10].

3.6 Pairwise features

Previous work has highlighted that the inclusion of information beyond raw four-vector data, such as pairwise features, can improve deep learning classifier performance [10, 27] in jet physics. Similarly, it is

³This class token is widely used in vision transformers. Particle Transformer follows the procedure of [30] to add the token only before the last few layers. We find that, even if the class token is fixed to a zero vector, the performance remains the same.

common practice to include high-level features in the training of BDTs to improve event classification, see e.g. [32]. The work of [27] suggests that this increase in performance is due to the resulting implicit embedding of Lorentz symmetry in the network architecture through features that adhere to (sub)symmetries. Lorentz symmetry has previously been shown to function as a strong inductive bias for neural network design [33–36].

For the BDT, we perform experiments with the inclusion of a variety of high-level features, which are treated on the same footing as the low-level ones. Similarly, we follow [10, 27] and include pairwise features in Particle Net and Particle Transformer through a trainable embedding U_{ij} for particles i and j . They are then included in Particle Net by replacing Equation (3.2) with

$$x'_i = \frac{1}{k} \sum_{j=1}^k \text{FCN}(x_i, x_i - x_{i_j} + U_{ij}) \quad (3.4)$$

and in Particle Transformer by replacing Equation (3.3) with

$$\text{Attention}(Q, K, T) = \text{SoftMax} \left(QK^T / \sqrt{d} + U \right) V. \quad (3.5)$$

In all three cases, we evaluated the performance of a wide variety of pairwise features, including m_{ij} , ΔR_{ij} , the jet-based features used in [10], three-body invariant masses, and discrete flavour interaction terms (i.e. a feature that is 1 when i and j are components of a SM current, and 0 otherwise). Using the feature importance indicator of the BDT, and empirically for Particle Net and Particle Transformer, we find that for all architectures the performance is saturated by the inclusion of only m_{ij} and ΔR_{ij} . Furthermore, the BDT indicates that we find that the pairwise invariant masses lead to the biggest gain in performance. This result is in line with the findings of [27].

4 Results

Our results are summarized in Table 3, which shows the area under the ROC curve (AUC) and the signal efficiency at background efficiencies of 1% and 10% for every method described above. Particle Net and Particle Transformer, both with pairwise features, were the best performing architectures across all performance metrics and all backgrounds. Between them, the performance is quite similar, with Particle Net slightly outperforming Particle Transformer in a few select cases. Note the significant outlier in the 1% signal efficiency in $t\bar{t} + W$, where Particle Transformer with pairwise features performs worse than most other architectures.

Figure 1 shows the ROC curves for all architectures and backgrounds and Figure 2 shows the output distributions of all classifiers. Note that, for the best-performing architectures, large parts of the background are concentrated at very small values of the classifier score. This is especially true for the background processes with the largest cross section, $t\bar{t} + W$ and $t\bar{t} + Z$. This attribute can help determine the backgrounds in the signal fits performed in the LHC experiments, since the bins with low score can determine the background processes.

The application of the best performing network architectures can improve the signal selection efficiency for a background efficiency by 10 – 30%. This improvement can be compared to that of an increase in statistical accuracy due to a larger integrated luminosity. Since this improvement scales with the square root of the increase in luminosity, the improvement in signal efficiency corresponds to a 30 – 50% increase in integrated luminosity. This is a huge factor, outlining the importance of modern machine learning techniques in particle physics analyses.

		BDT	BDT _{int.}	FCN	CNN
$t\bar{t} + h$	AUC	0.831(0)	0.838(0)	0.832(0)	0.834(3)
	$\epsilon_S(\epsilon_B = 0.1)$	0.560(2)	0.559(1)	0.557(0)	0.561(5)
	$\epsilon_S(\epsilon_B = 0.01)$	0.175(1)	0.175(9)	0.164(4)	0.222(7)
$t\bar{t} + W$	AUC	0.897(0)	0.899(0)	0.895(0)	0.888(2)
	$\epsilon_S(\epsilon_B = 0.1)$	0.714(1)	0.719(3)	0.710(1)	0.691(6)
	$\epsilon_S(\epsilon_B = 0.01)$	0.322(2)	0.311(7)	0.277(5)	0.321(14)
$t\bar{t} + WW$	AUC	0.745(0)	0.754(0)	0.743(0)	0.743(3)
	$\epsilon_S(\epsilon_B = 0.1)$	0.441(1)	0.451(1)	0.440(1)	0.438(8)
	$\epsilon_S(\epsilon_B = 0.01)$	0.108(2)	0.107(7)	0.107(2)	0.096(2)
$t\bar{t} + Z$	AUC	0.849(0)	0.868(0)	0.850(0)	0.856(1)
	$\epsilon_S(\epsilon_B = 0.1)$	0.597(2)	0.613(8)	0.585(3)	0.605(0)
	$\epsilon_S(\epsilon_B = 0.01)$	0.204(5)	0.234(8)	0.193(2)	0.226(6)
		PN	PN _{int.}	ParT	ParT _{int.}
$t\bar{t} + h$	AUC	0.851(0)	0.871(0)	0.843(0)	0.869(0)
	$\epsilon_S(\epsilon_B = 0.1)$	0.598(1)	0.643(0)	0.586(4)	0.646(6)
	$\epsilon_S(\epsilon_B = 0.01)$	0.221(8)	0.235(4)	0.213(5)	0.242(4)
$t\bar{t} + W$	AUC	0.901(0)	0.918(0)	0.901(0)	0.918(1)
	$\epsilon_S(\epsilon_B = 0.1)$	0.727(3)	0.761(2)	0.726(2)	0.767(2)
	$\epsilon_S(\epsilon_B = 0.01)$	0.338(4)	0.355(8)	0.333(10)	0.307(11)
$t\bar{t} + WW$	AUC	0.758(1)	0.791(0)	0.752(0)	0.790(0)
	$\epsilon_S(\epsilon_B = 0.1)$	0.451(2)	0.505(4)	0.448(2)	0.500(3)
	$\epsilon_S(\epsilon_B = 0.01)$	0.117(4)	0.125(3)	0.102(3)	0.123(11)
$t\bar{t} + Z$	AUC	0.875(2)	0.914(0)	0.866(0)	0.910(1)
	$\epsilon_S(\epsilon_B = 0.1)$	0.635(5)	0.716(1)	0.617(0)	0.711(3)
	$\epsilon_S(\epsilon_B = 0.01)$	0.242(10)	0.270(4)	0.218(6)	0.269(4)

Table 3. The area under the ROC curve and the signal efficiencies at background efficiency of 10% and 1%. Quoted uncertainty are extracted from three independent runs for every network architecture. Numbers in bold indicate the best performance. In case performance of multiple architectures are the best to within uncertainty, the results are both indicated.

Figure 3 shows the performance of Particle Net as a function of k , the number of nearest neighbours. As one might expect, performance improves with k , eventually saturating when k approaches the limit where every particle is connected to all other particles. Note that this limit would require more significant computational overhead in the context of jet physics, as the number of objects can grow much larger and the complexity scales like $\mathcal{O}(kn)$. Here, the number of objects is limited and setting $k = n$ is unproblematic. Note that this setup converts Particle Net into an architecture that is quite similar to Particle Transformer, as is reflected in the results.

5 Conclusions

In this work, we present an open dataset for the classification of four tops events from the SM background processes. We compared several state-of-the-art ML methods for supervised event classification, performing hyperparameter optimization for all of them. We found that the best-performing mod-

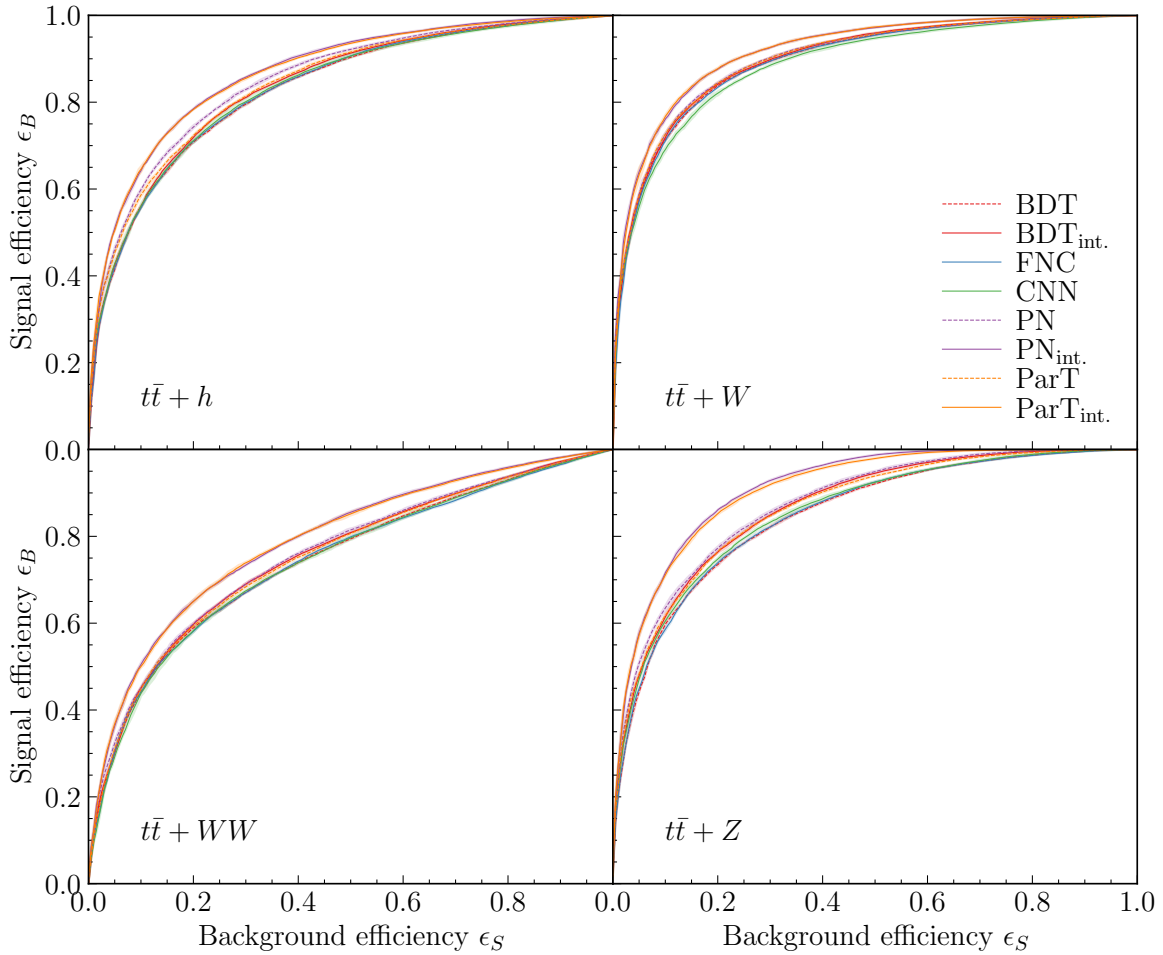


Figure 1. Receiver operating characteristic curves for all architectures on the four background processes. The solid lines and error bands correspond with the mean and standard deviation over three independent runs for every architecture.

els are Particle Net (PN) and the Particle Transformer (ParT) when pairwise features are included. Furthermore, when compared on individual background processes, we find that the best performance is obtained in $t\bar{t} + W$ and $t\bar{t} + Z$, which also have the largest cross section. In conclusion, we find an improvement in the signal efficiency ranging from 10% - 30% over our base models (BDT, FCN, CNN) and an increase by 5 - 15% over the particle net and transformer without pairwise features. This improvement in signal efficiency corresponds to a 30% - 50% increase in integrated luminosity. The application of better classifications can thus improve the signal efficiency for four tops production in the full analysis by comparable factors.

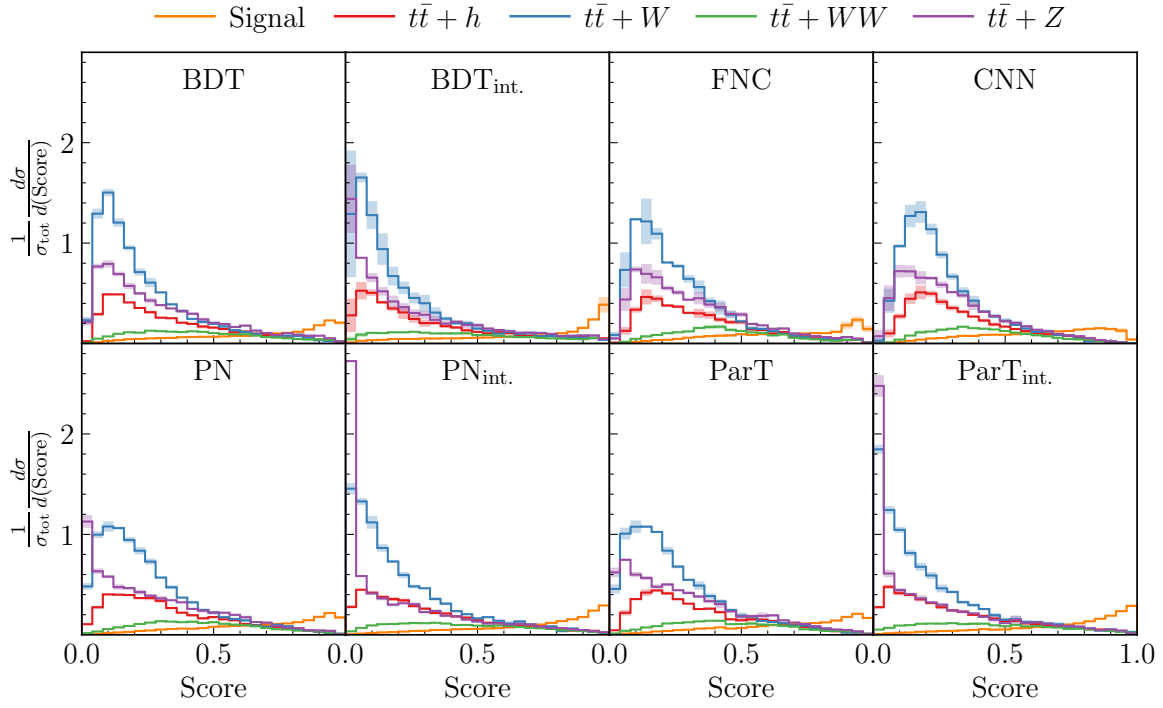


Figure 2. The distribution of the signal and the backgrounds as a function of the classifier score, normalized to the total cross section. The solid lines and error bands correspond with the mean and standard deviation over three independent runs for every architecture.

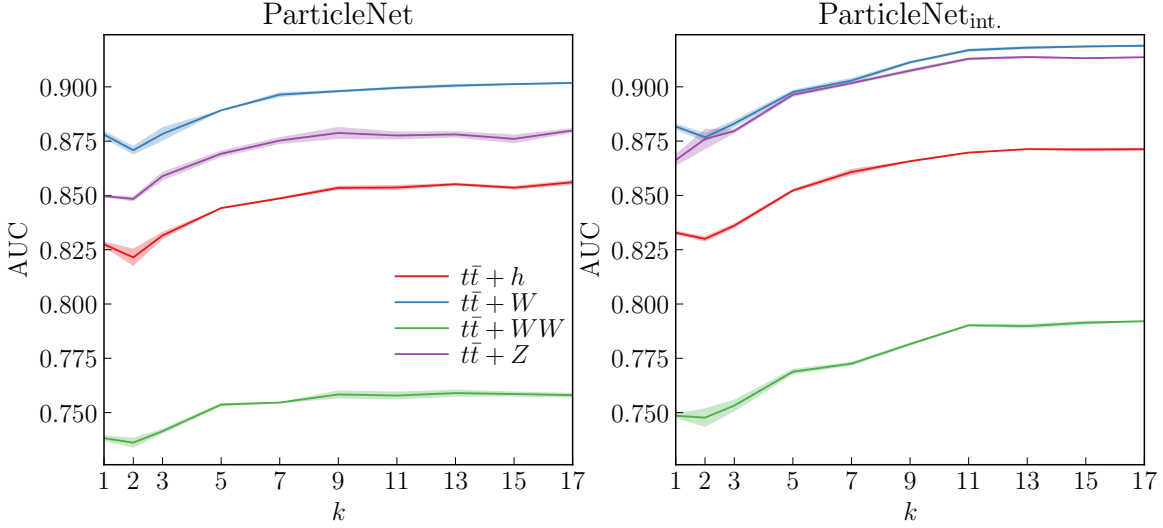


Figure 3. The performance of Particle Net on the four background processes as a function of k , the number of nearest neighbors. The solid lines and error bands correspond to the mean and standard deviation over three independent runs for every value of k .

Acknowledgements

The author(s) gratefully acknowledges the computer resources at Artemisa, funded by the European Union ERDF and Comunitat Valenciana as well as the technical support provided by the Instituto de Física Corpuscular, IFIC (CSIC-UV). R. RdA is supported by PID2020-113644GB-I00 from the Spanish Ministerio de Ciencia e Innovación. RV is supported by the European Research Council (ERC) under the European Union's Horizon 2020 research and innovation programme (grant agreement No. 788223, PanScales).

References

- [1] ATLAS collaboration, *Evidence for $t\bar{t}t\bar{t}$ production in the multilepton final state in proton–proton collisions at $\sqrt{s} = 13$ TeV with the ATLAS detector*, *Eur. Phys. J. C* **80** (2020) 1085 [[2007.14858](#)].
- [2] ATLAS collaboration, *Measurement of the $t\bar{t}t\bar{t}$ production cross section in pp collisions at $\sqrt{s} = 13$ TeV with the ATLAS detector*, *JHEP* **11** (2021) 118 [[2106.11683](#)].
- [3] CMS collaboration, *Search for production of four top quarks in final states with same-sign or multiple leptons in proton-proton collisions at $\sqrt{s} = 13$ TeV*, *Eur. Phys. J. C* **80** (2020) 75 [[1908.06463](#)].
- [4] A. Hocker et al., *TMVA - Toolkit for Multivariate Data Analysis*, [physics/0703039](#).
- [5] G. Karagiorgi, G. Kasieczka, S. Kravitz, B. Nachman and D. Shih, *Machine Learning in the Search for New Fundamental Physics*, [2112.03769](#).
- [6] Y. Coadou, *Boosted decision trees*, [2206.09645](#).
- [7] L. de Oliveira, M. Kagan, L. Mackey, B. Nachman and A. Schwartzman, *Jet-images — deep learning edition*, *JHEP* **07** (2016) 069 [[1511.05190](#)].
- [8] J. Shlomi, P. Battaglia and J.-R. Vlimant, *Graph Neural Networks in Particle Physics*, [2007.13681](#).
- [9] V. Mikuni and F. Canelli, *Point cloud transformers applied to collider physics*, *Mach. Learn. Sci. Tech.* **2** (2021) 035027 [[2102.05073](#)].
- [10] H. Qu, C. Li and S. Qian, *Particle Transformer for Jet Tagging*, [2202.03772](#).
- [11] J. Alwall, R. Frederix, S. Frixione, V. Hirschi, F. Maltoni, O. Mattelaer et al., *The automated computation of tree-level and next-to-leading order differential cross sections, and their matching to parton shower simulations*, *JHEP* **07** (2014) 079 [[1405.0301](#)].
- [12] NNPDF collaboration, *Parton distributions from high-precision collider data*, *Eur. Phys. J. C* **77** (2017) 663 [[1706.00428](#)].
- [13] T. Sjöstrand, S. Ask, J.R. Christiansen, R. Corke, N. Desai, P. Ilten et al., *An introduction to PYTHIA 8.2*, *Comput. Phys. Commun.* **191** (2015) 159 [[1410.3012](#)].
- [14] M.L. Mangano, M. Moretti, F. Piccinini, R. Pittau and A.D. Polosa, *ALPGEN, a generator for hard multiparton processes in hadronic collisions*, *JHEP* **07** (2003) 001 [[hep-ph/0206293](#)].
- [15] DELPHES 3 collaboration, *DELPHES 3, A modular framework for fast simulation of a generic collider experiment*, *JHEP* **02** (2014) 057 [[1307.6346](#)].
- [16] T. Aarrestad, M. van Beekveld, M. Bona, A. Boveia, S. Caron, J. Davies et al., *The dark machines anomaly score challenge: Benchmark data and model independent event classification for the large hadron collider*, *SciPost Physics* **12** (2022) .
- [17] T. Aarrestad et al., *The Dark Machines Anomaly Score Challenge: Benchmark Data and Model Independent Event Classification for the Large Hadron Collider*, *SciPost Phys.* **12** (2022) 043 [[2105.14027](#)].
- [18] G. Brooijmans et al., *Les Houches 2019 Physics at TeV Colliders: New Physics Working Group Report*, in *11th Les Houches Workshop on Physics at TeV Colliders: PhysTeV Les Houches*, 2, 2020 [[2002.12220](#)].
- [19] DarkMachines Community, “The 4tops dataset.” <https://doi.org/10.5281/zenodo.7277951>, November, 2022. 10.5281/zenodo.7277951.
- [20] S. Haykin, *Neural networks: a comprehensive foundation*, Prentice Hall PTR (1994).

- [21] D.P. Kingma and J. Ba, *Adam: A method for stochastic optimization*, *arXiv preprint arXiv:1412.6980* (2014) .
- [22] T. Akiba, S. Sano, T. Yanase, T. Ohta and M. Koyama, *Optuna: A next-generation hyperparameter optimization framework*, 2019. 10.48550/ARXIV.1907.10902.
- [23] G. Agarwal, L. Hay, I. Iashvili, B. Mannix, C. McLean, M. Morris et al., *Explainable ai for ml jet taggers using expert variables and layerwise relevance propagation*, 2020. 10.48550/ARXIV.2011.13466.
- [24] CMS collaboration, *Identification of heavy, energetic, hadronically decaying particles using machine-learning techniques*, *Journal of Instrumentation* **15** (2020) P06005.
- [25] H. Qu and L. Gouskos, *ParticleNet: Jet Tagging via Particle Clouds*, *Phys. Rev. D* **101** (2020) 056019 [[1902.08570](#)].
- [26] Y. Wang, Y. Sun, Z. Liu, S.E. Sarma, M.M. Bronstein and J.M. Solomon, *Dynamic graph cnn for learning on point clouds*, *ACM Trans. Graph.* **38** (2019) .
- [27] C. Li, H. Qu, S. Qian, Q. Meng, S. Gong, J. Zhang et al., *Does Lorentz-symmetric design boost network performance in jet physics?*, [2208.07814](#).
- [28] Hqucms/weaver, *Streamlined neural network training*, <https://github.com/hqucms/weaver>.
- [29] A. Vaswani, N. Shazeer, N. Parmar, J. Uszkoreit, L. Jones, A.N. Gomez et al., *Attention is all you need*, *CoRR* **abs/1706.03762** (2017) [[1706.03762](#)].
- [30] H. Touvron, M. Cord, A. Sablayrolles, G. Synnaeve and H. Jégou, *Going deeper with image transformers*, *CoRR* **abs/2103.17239** (2021) [[2103.17239](#)].
- [31] Jet-universe/particle_transformer, *Official implementation of "particle transformer for jet tagging"*, https://github.com/jet-universe/particle_transformer.
- [32] M. Drees, M. Shi and Z. Zhang, *Machine Learning Optimized Search for the Z' from $U(1)_{L_\mu - L_\tau}$ at the LHC*, [2109.07674](#).
- [33] A. Butter, G. Kasieczka, T. Plehn and M. Russell, *Deep-learned Top Tagging with a Lorentz Layer*, *SciPost Phys.* **5** (2018) 028 [[1707.08966](#)].
- [34] M. Erdmann, E. Geiser, Y. Rath and M. Rieger, *Lorentz Boost Networks: Autonomous Physics-Inspired Feature Engineering*, *JINST* **14** (2019) P06006 [[1812.09722](#)].
- [35] A. Bogatskiy, B. Anderson, J.T. Offermann, M. Roussi, D.W. Miller and R. Kondor, *Lorentz Group Equivariant Neural Network for Particle Physics*, [2006.04780](#).
- [36] S. Gong, Q. Meng, J. Zhang, H. Qu, C. Li, S. Qian et al., *An efficient Lorentz equivariant graph neural network for jet tagging*, *JHEP* **07** (2022) 030 [[2201.08187](#)].